Original research

Residual tumour detection in post-treatment granulation tissue by using advanced diffusion models in head and neck squamous cell carcinoma patients

Abbreviations:

ADC, apparent diffusion coefficient

AUC, area under curve

DDC, distributed diffusion coefficient

DKI, diffusion kurtosis imaging

DWI, diffusion-weighted image

EPI, echo-planar imaging

HNSCC, head and neck squamous cell carcinoma

IVIM, intravoxel incoherent motion

ROC, receiver operating characteristic

ROI, region of interest

SDM, statistical diffusion model

SEM, stretched exponential model

ABSTRACT

Purpose: To evaluate the detectability of the residual tumour in post-treatment granulation tissue using parameters obtained with an advanced diffusion model in patients with head and neck squamous cell carcinoma (HNSCC) treated by chemoradiation therapy.

Materials and Methods: We retrospectively evaluated 23 patients with HNSCC after the full course of chemoradiation therapy. The diffusion-weighted image (DWI) acquisition used single-shot spin-echo echo-planar imaging with 11 b-values (0–1000). We calculated 10 DWI parameters using a mono-exponential model, a bi-exponential model, a stretched exponential model (SEM), a diffusion kurtosis imaging (DKI) model and a statistical diffusion model (SDM) in the region of interest (ROI) placed on the post-treatment granulation tissue. The presence of residual tumour was determined by histological findings or clinical follow-up.

Results: Among the 23 patients, seven patients were revealed to have residual tumour. The univariate analysis revealed significant differences in six parameters between the patients with and without residual tumour. From the receiver operating characteristic curve analysis, the highest area under curve was detected in the center of the Gaussian distribution of diffusion coefficient (D_s) obtained by the SDM. The multivariate

analysis revealed that the D_s and diffusion heterogeneity (α) obtained by the SEM were predictors for the presence of residual tumour.

Conclusion: DWI parameters obtained by advanced fitting models will be one of the diagnostic tools for the detection of residual tumour.

Keywords:

Diffusion weighted imaging, advanced diffusion model, residual tumour, post-treatment granulation tissue, head and neck squamous cell carcinoma,

Introduction

Surgical resection, chemotherapy, radiotherapy, and their combinations are common treatments for head and neck squamous cell carcinoma (HNSCC) [1]. In particular, the use of super-selective arterial infusions of cisplatin with concomitant radiotherapy has become popular for head and neck SCC because of its higher local control rate in advanced cases, especially those in the nasal or sinonasal cavity, oral cavity and pharynx SCCs [2–4].

After nonsurgical treatment, the presence or absence of residual tumour must be determined before selecting the next treatment — such as additional surgical resection and chemotherapy — or deciding the details of a follow-up strategy. Although computed tomography (CT) and magnetic resonance imaging (MRI) have been widely used to evaluate the presence of residual tumour tissue, these modalities mainly achieve a morphological evaluation only, and thus it is often difficult to distinguish whether or not post-treatment granulation tissue contains residual tumour [5]. As another method, positron-emission tomography (PET) with 18F-fluorodeoxyglucose (FDG) is widely used for the detection of residual tumour by depicting the high glucose metabolism of residual tumour [6]. However, especially at the early time point after the treatment, post-treatment inflammatory changes (particularly in the sinonasal cavity) cause FDG

uptake by their biological activity due to inflammation, which makes it difficult to distinguish post-treatment granulation and residual tumour, resulting in a failure to detect residual tumour in post-treatment granulation tissue [7]. In such post-treatment granulation tissue, the microstructure is thought to contain the post-treatment inflammatory or granulation tissue, but if a certain amount of residual tumour tissue is present, the microstructural characteristics may be different compared to those of only inflammatory granulation tissue. The details of tissue microstructure can be assessed using diffusion-weighted imaging (DWI), which reveals the micro-water diffusion; this indirectly reflects aspects of the microstructural architecture such as the cell membrane [8]. Compared to the conventional model of the apparent diffusion coefficient (ADC) obtained by mono-exponential fitting, multiple advanced models have been reported to well reflect the complicated signal decay of multiple b-value data in DWI [9–12]. Such advanced models can reflect the microstructural information in greater detail and may detect residual tumour in post-treatment granulation tissues.

We conducted the present study to evaluate the detectability of residual tumour in post-treatment granulation tissue, using parameters obtained with multiple advanced diffusion models in HNSCC patients treated with chemoradiation.

Materials and Methods

Patients

The protocol of this retrospective study was approved by our institutional review board, and written informed consent was waived. We evaluated the cases of 23 patients with HNSCC who were treated at our hospital during the roughly 3-year period from September 2012 to February 2015. All patients fulfilled the following inclusion criteria: (1) histopathological diagnosis of SCC, (2) the patient had undergone a full course of curative treatment with 70-Gy radiation, and (3) MRI including multiple b-value DWI was performed within 1 month after the end of the full course of treatment. The characteristics of the 23 patients were as follows: 19 males and four females (mean age 59.5 yrs, range 47–73 yrs). The primary lesions involved the maxillary sinus in 20 patients and the nasal cavity in three patients. The histopathological diagnoses were SCC in all patients. The T stage was T3 in nine patients, T4a in 10, and T4b in four. The treatment regimen was a super-selective arterial infusion of cisplatin with concomitant radiotherapy for all patients. The patients' treatment details were as follows: an arterial infusion of cisplatin (100–120 mg/m^2 per week for 4 weeks) to the primary tumour's dominant blood supply, using a microcatheter, with concurrent radiotherapy of a total of 70 Gy in 35 fractions. MRI scans including multi b-value scanning were performed in

all patients within 1 month after the full course of treatment. The time interval between the end of treatment and the MRI scanning was 13–21 days (15.1±1.8 days).

Clinical assessment

In all patients, clinical and radiological follow-ups were performed after the treatment to determine the final diagnosis related to the presence of residual tumour at the primary site. The presence of residual tumour was determined by the histopathological confirmation of SCC by biopsy or surgical resection, the development of a mass lesion in the post-treatment granulation tissue, or the definite enlargement of granulation tissue area during the follow-up, which was ≥ 1 year (the minimum follow-up period was set as 1 year). The non-presence of residual tumour was determined by histopathological confirmation of the absence of SCC by surgical resection, the absence of enlargement of the suspected lesion of the residual tumour, or the absence of a new lesion in the post-treatment granulation tissue within the follow-up period.

Imaging protocols

All MR imaging was performed using a 3.0 Tesla unit (Achieva TX; Philips

Healthcare, Best, Netherlands) with a 16-channel neurovascular coil. The DWI acquisition used single-shot spin-echo echo-planar imaging (EPI) with three orthogonal motion probing gradients. Eleven b-values (0, 10, 20, 30, 50, 80, 100, 200, 400, 800 and 1000 s/mm^2) were used. The other imaging parameters were: TR, 4500 ms; TE, 64 ms; DELTA (large delta; gradient time interval), 30.1 ms; delta (small delta; gradient duration), 24.3 ms; flip angle, 90°; field of view (FOV), 230×230 mm; 64×64 matrix; slice thickness, 5 mm×20 slices; voxel size 3.59×3.59×5.00 mm; parallel imaging acceleration factor, 2; the number of signal averages = b-value of 0–100 s/mm^2 (one average), 200–800 s/mm^2 (two averages) and 1000 s/mm^2 (three averages); scanning time, 4 min 02 s.

Conventional MR images were also obtained to evaluate the primary tumour. These images included (a) axial T1-weighted image (T1WI) with a spin-echo sequence (TR, 450 ms; TE, 10 ms; FOV, 240×240 mm; 512×512 matrix; slice thickness, 5 mm; inter-slice gap, 30%; scanning time, 2 min 12 s), and (b) axial T2-weighted image (T2WI) with a turbo spin-echo (TSE) sequence with fat suppression (TR, 4500 ms; TE, 70 ms; TSE factor, 9; FOV, 240×240 mm; 512×512 matrix; slice thickness, 5 mm; inter-slice gap, 30%; scanning time, 2 min 06 s).

Data analysis

ROI settings

For the region of interest (ROI) delineation, a board-certified neuroradiologist with 19 years of experience delineated each post-treatment granulation tissue with a polygonal ROI on b0 images; axial T1WI and T2WI were used as reference images (Fig.1). By referring to the region where the primary tumor was present before the treatment, the abnormal soft tissue that was suspected to contain post-treatment granulation tissue and/or residual tumor was identified by using the T1WI and T2WI imaging findings. Such tissue was considered to present a typically slightly high or intermediate signal on T2WI with a low signal on T1WI and was different from the normal anatomical structure. The post-treatment granulation tissue did not show strong high signal intensity on T2WI that suggested inflammatory tissue (such as thickened mucosa or fluid correction) or high signal intensity on T1WI, which suggested the subacute hemorrhage or mutinous fluid, and thus such region was excluded.. The ROI was then delineated so that it contained only the post-treatment granulation tissue on the b0 image with the reference information mentioned above. Mainly the T2WI image in particular was used, because the image contrast of T2WI was almost the same as the b0 image of the conventional EPI. If the granulation tissue extended into two or more slices,

all slices in which the tumour was included were used for the ROI delineation. Each delineated tumour ROI was copied on each b-value image. The signal intensity in each b-value image was determined as the mean value in the delineated ROI by integrating all granulation tissue voxels from all delineated slices into the total signal intensity. The data analysis was performed using this ROI-based mean value (not a pixel-by-pixel basis) for the maintenance of a sufficient signal-to-noise ratio (SNR), as reported in an investigation using an intravoxel incoherent motion (IVIM) analysis [11].

Diffusion data calculation

From the diffusion signal data obtained by the ROI analysis, we calculated each parameter of the mono-exponential function (here, the ADC), the bi-exponential function (the perfusion fraction f, the pseudo-diffusion coefficient D*, and the slow diffusion coefficient D), and the parameters for the diffusion kurtosis imaging (DKI) (the kurtosis value K and the kurtosis-corrected diffusion coefficient D_k), the stretched exponential model (SEM) (diffusion heterogeneity α and the distributed diffusion coefficient DDC) and the statistical diffusion model (SDM) (the width of the Gaussian distribution σ and the center of the Gaussian distribution of diffusion coefficient D_s) . Using the signal intensity of all 11 b-values, we calculated the bi-exponential function

parameters. Because assessments of the ADC, DKI, SEM and SDM usually targeted the tissue diffusion except for the perfusion-related signal, we used the signal intensity of five b-values (0, 200, 400, 800 and 1000 s/mm^2) for the parameter calculation of the ADC, DKI, SEM and SDM. To perform these parameter calculations, we used the following equations [9–12]:

$$\frac{S_{(b)}}{S_0} = e^{-b \cdot ADC} \tag{1}$$

$$\frac{S_{(b)}}{S_0} = f \cdot e^{-b \cdot D^*} + (1 - f) \cdot e^{-b \cdot D} \tag{2}$$

$$\frac{S_{(b)}}{S_0} = \exp\left[-b * D_k + \frac{1}{6} * b^2 * {D_k}^2 * K \right] \tag{3}$$

$$\frac{S_{(b)}}{S_0} = e^{-(b \cdot DDC)^{\alpha}} \tag{4}$$

$$\frac{S_{(b)}}{S_0} = \frac{1 + \phi\left(\frac{D_s}{\sigma\sqrt{2}} - \frac{b\sigma}{\sqrt{2}} \right)}{1 + \phi\left(\frac{D_s}{\sigma\sqrt{2}} \right)} e^{-(b \cdot D_s + \frac{1}{2} b^2 \sigma^2)} \tag{5}$$

where $S_{(b)}$ is the signal intensity at the b-value denoted by the subscript, S_0 is the signal intensity at the b-value of 0, and b is the b-factor in Eqs. (1) to (5). The ϕ in Eq. (5) denotes the error function described in the previous report [12]. We fitted the signal

intensity of b-values in Eqs. (1) to (5) with least square fitting using the Levenberg-Marquardt algorithm.

Statistical analysis

In a univariate analysis, we used the Mann-Whitney U-test to compare the values of ADC, f, D*, D, K, D_k, α, DDC, σ and D_s between the post-treatment granulation tissues with and without residual tumour, respectively. If a significant difference was obtained for more than two parameters among all parameters, these parameters were analyzed by multivariate logistic regression models to determine whether they had independent predictive value with odds ratios (OR) and corresponding 95% confidence intervals (CIs). The detected predictive values were also assessed using receiver operating characteristic (ROC) curves constructed for calculating the area under the curve (AUC). We determined the sensitivity, specificity, positive predictive value, negative predictive value and diagnostic accuracy by using the closest point to the upper left corner of the ROC curve in the division of the post-treatment granulation tissues with and without residual tumour. P-values <0.05 were considered significant. SPSS software (IBM, Armonk, NY) was used for all analyses.

Results

We successfully obtained DWI parameters for all post-treatment granulation tissues. Among the 23 patients, seven were found to have residual tumour. The residual tumour of six patients was confirmed by histopathological findings. One residual tumour and 16 granulation tissues without residual tumour were determined by clinical diagnosis at follow-up (mean 21 mos; range 13–47 mos). All of the parameter data are presented in Table 1.

The univariate analysis revealed significant differences between the local control and failure groups in ADC, D, D_k, DDC, α and D_s, respectively. The K values tended to be different, but not significantly so (p=0.08). From the ROC curve analysis, the AUC, sensitivity, specificity, positive predictive value, negative predictive value, accuracy and cut-off value were calculated (Table 2). The parameter with the highest AUC was the D_s value obtained by the SDM.

The multivariate analysis revealed that the D_s and α were independent predictors for determining the presence of residual tumour (Table 3).

Discussion

We successfully determined the multiple models' diffusion parameters in all post-treatment granulation tissues. In the residual tumour group, the detectability of D_s obtained by the SDM may be the best, based on the AUC revealed by the ROC curve analysis, although the slow diffusion coefficient D from the bi-exponential model has the same degree of diagnostic accuracy. In addition, D_s obtained by the SDM and α by the SEM were both shown to be independent predictors for the detection of residual tumour.

Another report described the utility of 18F-FDG PET/CT scanning for the detection of residual tumor after curative chemoradiation therapy in HNSCC patients [6]. However, especially in the nasal cavity and sinonasal sinus, the FDG uptake in the post-treatment inflammation is problematic for the detection of residual tumor, and thus clinicians should wait until the inflammation becomes inactive; it will be a long time before the residual tumor can be clearly detected. In comparison, our present findings can be used to help detect residual tumor even in the early period after treatment. Being able to predict the presence of residual tumor in post-treatment granulation tissue will provide useful information for decision-making regarding the need for additional chemotherapy and the planning of earlier salvage surgery after the current chemoradiotherapy. This information will also contribute to the determination of a

follow-up strategy, such as the determination of the interval for CT or MR scanning. These contributions can improve the quality of patient care in post-treatment follow-up.

Several studies have shown the usefulness of the ADC obtained by mono-exponential fitting for detecting residual or recurrent tumour in HNSCC. Most studies have reported that a lower ADC was characteristic in post-treatment granulation tissue that includes residual tumour [13–15]. Although our present findings also indicated the utility of the ADC value in the differentiation of post-granulation tissue with and without residual tumour, there was a large overlap resulting in the lower AUC value in the ROC analysis, which made the determination of the presence of residual tumour difficult. We suspect that the reason for this is that the ADC value obtained by the simple mono-exponential fitting model cannot represent the complicated microstructure of post-treatment granulation tissue that may include inflammation tissue, micro-necrosis, fibrous tissue, tissue related to the microcirculation, and residual tumour.

A limited number of studies have used a non-linear fitting model for the DWI signal decay curve in the post-treatment granulation tissue of head and neck cancer [16–18], and no study has compared the use of DKI, SEM, and SDM, to our knowledge. Mao et al. reported that the slow water-related diffusion coefficient D and the perfusion

fraction f obtained by bi-exponential fitting were significant parameters for the differentiation of post-treatment granulation with and without residual tumour, and that D in particular has very high diagnostic accuracy for the differentiation [16]. The target histological type in the Mao et al. study, i.e., undifferentiated cancer of the nasopharynx was different from the target of our study. However, our present findings indicate the same trend as that reported by Mao et al.: the slow diffusion coefficient D from bi-exponential fitting has good diagnostic accuracy and was superior to the mono-exponential model of ADC. Moreover, our present findings indicated that the diagnostic accuracy of D_s obtained by the SDM was the same as that of the D obtained by bi-exponential fitting. We suspect that the microstructural complexity provided by the presence of residual tumour tissue (which is represented by restricted water diffusion due to the high cellular density and complex distribution of the cell membrane) will be well reflected by the complex fitting model of the advanced DWI model. In contrast, Tshering Vogel et al. found that the slow diffusion coefficient D and the perfusion fraction f obtained by a bi-exponential fitting model were both significant parameters for the differentiation of post-treatment tissue with and without residual tumour in patients with laryngeal or hypopharyngeal SCC treated by chemoradiation [17]. However, the most powerful predictor they identified was the perfusion fraction f,

not the slow diffusion coefficient D. The reason for this discrepancy with our study is difficult to explain. We suspect that it may be due to the difference in the distribution of b-value data, differences in the post-procession parameter calculation methods, and/or the difference in the primary site of SCC.

Additionally, although its diagnostic accuracy was not superior to that of the ADC, the diffusion heterogeneity parameter α obtained by the stretched exponential model was revealed as an independent predictor for the determination of residual tumour by our multiple logistic regression analysis. This parameter might have a somewhat different biological meaning compared to a diffusion coefficient value such as the ADC, D, D_k, DDC and D_s. The α was considered to reflect the diffusion heterogeneity, which reflected the degree of difference from the signal decay derived by the Gaussian distribution of water diffusion [19], whereas the value of the diffusion coefficient is thought to reflect the degree of signal decay between the signal intensity of different b-value data. The combination of these parameters of diffusion coefficient and diffusion heterogeneity can reveal more details of post-granulation tissue characteristics. However, these advanced diffusion models provide only the mathematical aspects, and it is unclear which histological tissue characteristics are reflected by these parameters. It is thus necessary to conduct further studies to

determine the slice-to-slice and spot-to-spot correlations between histological tissue and these diffusion parameters.

The present study has several limitations. It was a retrospective study, and thus a fixed b-value was used only for the diffusion signal analysis. Although we used low (b=0–100), medium (b=100–400) and high (b=800–1000) b-values for the signal analysis in this study, the appropriate arrangement of b-values for the short scanning time with sufficient reliability was not unclear. The reduction of the b-value for shortening the scan time while maintaining the reliability of the calculated parameters should be assessed in a future study. Cramer-Rao's lower bound theory was described to minimize the number of b-values required for a suitable quantification [20], and such a technique can be useful for the b-value optimization. Second, we investigated the diagnostic power of DWI parameters only; a direct comparison with other modalities for the assessment of the superiority of diagnostic accuracy was not conducted. Imaging characteristics such as the MR T1- or T2-weighted image signal intensity, the pattern of contrast enhancement, and the shape of granulation tissue will be helpful for the detection of residual tumour [21]. However, the interpretation of these imaging findings differs among radiologists with various types of levels of experience, and even an expert radiologist may miss the diagnosis of residual tumour because there is a wide variety of

imaging findings in post-treatment tissue. However, diffusion parameters are quantitative, and their interpretation will be easier than that of imaging findings. Third, we used a scan protocol with only a single scanning session at the early phase after the treatment. In the follow-up, the post-treatment granulation tissue had changed from inflammatory granulation to fibrous tissue. The difference in diffusion characteristics between residual tumor and fibrous granulation was still unclear. In addition, the diffusion parameters' tendency to show time-course changes in granulation tissue with and without residual tumor was also unclear. These issues will be addressed in a future analysis.

In conclusion, advanced diffusion fitting models will be one of the diagnostic tools for the detection of residual tumour in post-treatment granulation. This finding can contribute to the planning of additional surgical resection or chemotherapy after chemoradiation therapy and to the selection of follow-up strategies.

References

[1] Wong SJ, Harari PM, Garden AS, Schwartz M, Bellm L, Chen A, Curran WJ, Murphy BA, Ang KK, Longitudinal Oncology Registry of Head and Neck Carcinoma (LORHAN): analysis of chemoradiation treatment approaches in the United States. Cancer. 117 (2011) 1679-1686.

[2] Homma A, Oridate N, Suzuki F, Taki S, Asano T, Yoshida D, Onimaru R, Nishioka T, Shirato H, Fukuda S, Superselective high-dose cisplatin infusion with concomitant radiotherapy in patients with advanced cancer of the nasal cavity and paranasal sinuses: a single institution experience. Cancer. 115 (2009) 4705-4714.

[3] Homma A, Sakashita T, Yoshida D, Onimaru R, Tsuchiya K, Suzuki F, Yasuda K, Hatakeyama H, Furusawa J, Mizumachi T et al., Superselective intra-arterial cisplatin infusion and concomitant radiotherapy for maxillary sinus cancer. Br J Cancer. 109 (2013) 2980-2986.

[4] Kano S, Homma A, Oridate N, Suzuki F, Hatakeyama H, Mizumachi T, Furusawa J, Sakashita T, Yoshida D, Onimaru R et al., Superselective arterial cisplatin infusion with concomitant radiation therapy for base of tongue cancer. Oral Oncol. 47 (2011) 665-670.

[5] Fujima N, Kudo K, Yoshida D, Homma A, Sakashita T, Tsukahara A, Khin Khin T,

Yuri Z, Satoshi T, Hiroki S, Arterial spin labeling to determine tumor viability in head and neck cancer before and after treatment. J Magn Reson Imaging. 40 (2014) 920-928.

[6] Tantiwongkosi B, Yu F, Kanard A, Miller FR, Role of (18)F-FDG PET/CT in pre and post-treatment evaluation in head and neck carcinoma. World J Radiol. 6 (2014) 177-191.

[7] McCollum AD, Burrell SC, Haddad RI, Norris CM, Tishler RB, Case MA, Posner MR, Van den Abbeele AD, Positron emission tomography with 18F-fluorodeoxyglucose to predict pathologic response after induction chemotherapy and definitive chemoradiotherapy in head and neck cancer. Head Neck. 26 (2004) 890-896.

[8] Eida S, Van Cauteren M, Hotokezaka Y, Katayama I, Sasaki M, Obara M, Okuaki T, Sumi M, Nakamura T, Length of intact plasma membrane determines the diffusion properties of cellular water. Scientific Reports. 6 (2016) 19051.

[9] Chen Y, Ren W, Zheng D, Zhong J, Liu X, Yue Q, Liu M, Xiao Y, Chen W, Chan Q et al., Diffusion kurtosis imaging predicts neoadjuvant chemotherapy responses within 4 days in advanced nasopharyngeal carcinoma patients. J Magn Reson Imaging. 42 (2015) 1354-1361.

[10] Fujima N, Yoshida D, Sakashita T, Homma A, Tsukahara A, Shimizu Y, Tha KK, Kudo K, Shirato H, Prediction of the treatment outcome using intravoxel incoherent motion and diffusional kurtosis imaging in nasal or sinonasal squamous cell carcinoma patients. Eur Radiol. 2016. Jun 2. [Epub ahead of print].

[11] Fujima N, Yoshida D, Sakashita T, Homma A, Tsukahara A, Tha KK, Kudo K, Shirato H, Intravoxel incoherent motion diffusion-weighted imaging in head and neck squamous cell carcinoma: assessment of perfusion-related parameters compared to dynamic contrast-enhanced MRI. Mag Res Imaging. 32 (2014) 1206-1213.

[12] Yuan J, Yeung DK, Mok GS, Bhatia KS, Wang YX, Ahuja AT, King AD: Non-Gaussian analysis of diffusion weighted imaging in head and neck at 3T: a pilot study in patients with nasopharyngeal carcinoma. PloS One. 9 (2014) e87024.

[13] Vandecaveye V, De Keyzer F, Dirix P, Lambrecht M, Nuyts S, Hermans R: Applications of diffusion-weighted magnetic resonance imaging in head and neck squamous cell carcinoma. Neuroradiology. 52 (2010) 773-784.

[14] Vandecaveye V, de Keyzer F, Vander Poorten V, Deraedt K, Alaerts H, Landuyt W, Nuyts S, Hermans R, Evaluation of the larynx for tumour recurrence by diffusion-weighted MRI after radiotherapy: initial experience in four cases. Br J

Radiol. 79 (2006) 681-687.

[15] Vandecaveye V, Dirix P, De Keyzer F, Op de Beeck K, Vander Poorten V, Hauben E, Lambrecht M, Nuyts S, Hermans R, Diffusion-weighted magnetic resonance imaging early after chemoradiotherapy to monitor treatment response in head-and-neck squamous cell carcinoma. Int. J. Radiat. Oncol. Biol. Phys. 82 (2012) 1098-1107.

[16] Mao J, Shen J, Yang Q, Yu T, Duan X, Zhong J, Phuyal P, Liang B, Intravoxel incoherent motion MRI in differentiation between recurrent carcinoma and postchemoradiation fibrosis of the skull base in patients with nasopharyngeal carcinoma. J Magn Reson Imaging 2016. May 26. doi: 10.1002/jmri.25302. [Epub ahead of print].

[17] Tshering Vogel DW, Zbaeren P, Geretschlaeger A, Vermathen P, De Keyzer F, Thoeny HC, Diffusion-weighted MR imaging including bi-exponential fitting for the detection of recurrent or residual tumour after (chemo)radiotherapy for laryngeal and hypopharyngeal cancers. Eur Radiol. 23 (2013) 562-569.

[18] Lai V, Li X, Lee VH, Lam KO, Chan Q, Khong PL, Intravoxel incoherent motion MR imaging: comparison of diffusion and perfusion characteristics between nasopharyngeal carcinoma and post-chemoradiation fibrosis. Eur Radiol. 23 (2013)

2793-2801.

[19] Bennett KM, Hyde JS, Schmainda KM, Water diffusion heterogeneity index in the human brain is insensitive to the orientation of applied magnetic field gradients. Magn Reson Med Sci. 56 (2006) 235-239.

[20] Leporq B, Saint-Jalmes H, Rabrait C, Pilleul F, Guillaud O, Dumortier J, Scoazec JY, Beuf O, Optimization of intra-voxel incoherent motion imaging at 3.0 Tesla for fast liver examination. J Magn Reson Imaging. 41 (2015) 1209-1217.

[21] Sugimura K, Kuroda S, Furukawa T, Matsuda S, Yoshimura Y, Ishida T, Tongue cancer treated with irradiation: assessment with MR imaging. Clin Radiol. 46 (1992) 243-247.

Table and Figure captions

Table 1: DWI parameters of post-granulation tissue in all 23 patients

	Local Control	Local Failure
Mono-exponential model		
ADC	2.09±0.23	1.85±0.23
Bi-exponential model		
f	0.18±0.08	0.18±0.1
D*	14.2±5.78	14.1±8.2
D	1.76±0.19	1.48±0.18
Kurtosis model		
K	0.61±0.17	0.73±0.12
D_k	2.43±0.28	2.09±0.26
Stretched exponential model		
α	0.78±0.1	0.69±0.08
DDC	2.12±0.29	1.88±0.18
Statistical model		
D_s	1.02±0.13	0.83±0.09
σ	2.15±0.73	1.81±0.63

Table 1 footnote: Data are mean ± SD. ADC: apparent diffusion coefficient ($\times 10^{-3}$ mm^2/s), D: slow diffusion coefficient ($\times 10^{-3}$ mm^2/s), f: perfusion fraction ($\times 10^{2}$ %), D*: pseudo diffusion coefficient ($\times 10^{-3}$ mm^2/s), K: kurtosis value (dimensionless), D_k: kurtosis-corrected diffusion coefficient ($\times 10^{-3}$ mm^2/s), α: diffusion heterogeneity (dimensionless), DDC: distributed diffusion coefficient ($\times 10^{-3}$ mm^2/s), σ:

width of the Gaussian distribution ($\times 10^{-3}$ mm^2/s), D_s: the center of the Gaussian distribution of the diffusion coefficient ($\times 10^{-3}$ mm^2/s).

Table 2: The Results of ROC analysis

Parameter	AUC	Sensitivity	Specificity	PPV	NPV	Accuracy	Cut-off value
ADC	0.78	0.71	0.75	0.56	0.86	0.74	1.85
D	0.84	1	0.75	0.64	1	0.83	1.65
D_k	0.81	0.57	0.88	0.67	0.82	0.78	2.05
α	0.74	1	0.63	0.54	1	0.74	0.76
DDC	0.75	0.71	0.75	0.56	0.86	0.74	1.85
D_s	0.89	0.71	0.88	0.71	0.88	0.83	0.91

Table 2 footnote: AUC: area under curve, PPV: positive predictive value, NPV: negative predictive value.

Table 3: Significant Parameters in Multivariate Logistic Regression Models

Parameter	Odds ratio	P-value
α	0.91 (0.85, 0.96)	>0.05
Ds	2.24 (1.16, 4.11)	>0.01

Table 3 footnote: Data are odds ratios and p-values. Data in parentheses are 95% confidence intervals.

Fig. 1. ROI delineation on post-treatment granulation tissue. Each tumour ROI was delineated on a DWI image (b=0) corresponding to the post-granulation tissue with a polygonal ROI (a; arrow). An axial T1WI (b) and T2WI (c) were used as reference images for the supporting tool of ROI delineation.

Figure 1a

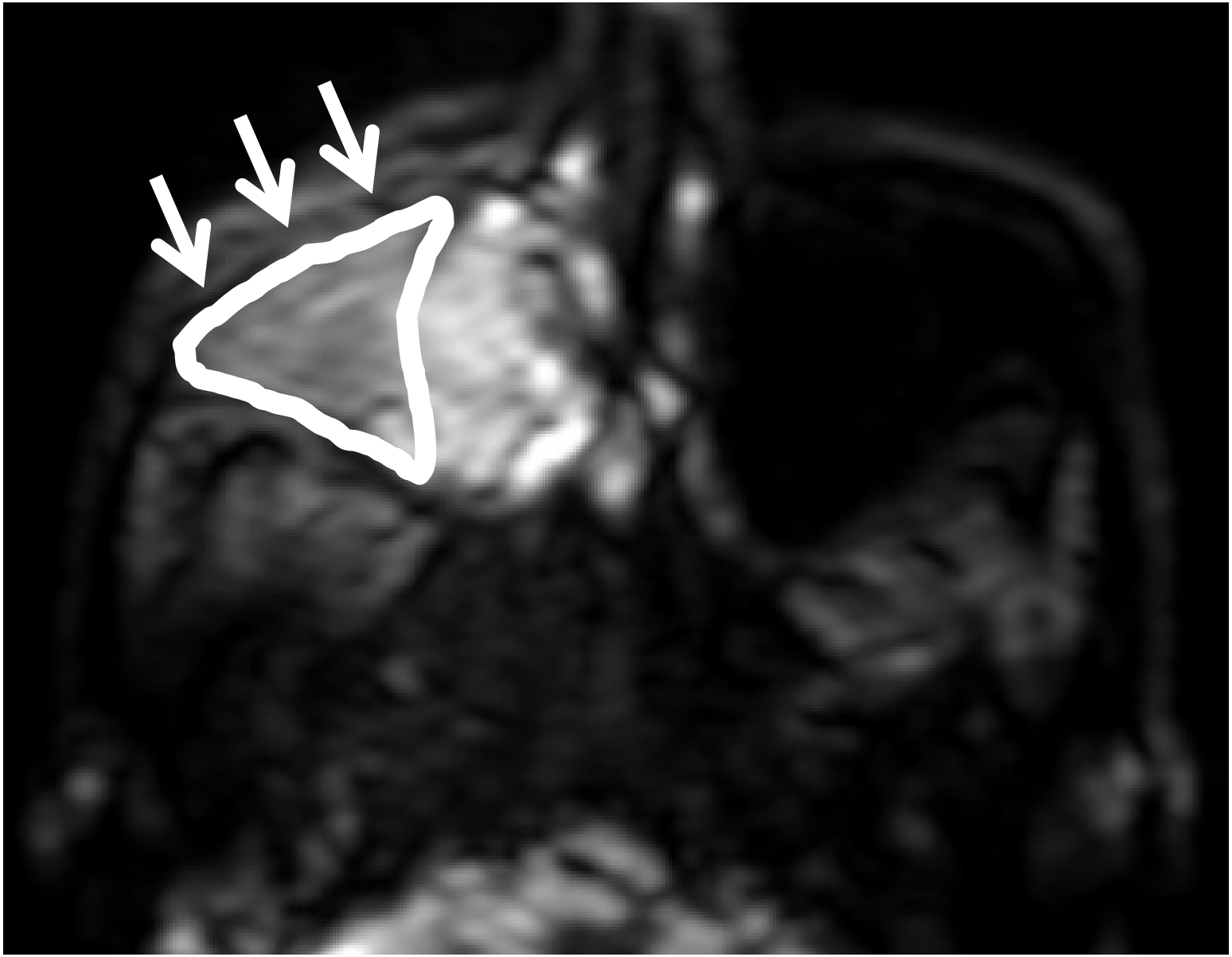

Figure 1b

Figure 1c